EFFECT OF LASER INDUCED CRYSTALLINITY MODIFICATION ON BIODEGRADATION PROFILE OF POLY(L-LACTIC ACID)

M204

Shan-Ting Hsu, Huade Tan, Y. Lawrence Yao

Department of Mechanical Engineering, Columbia University
New York, NY, 10027, USA

Abstract

The biodegradable and biocompatible polymer such as poly(L-lactic acid) (PLLA) is promising in drug delivery applications, while its induction period of biodegradation prevents the embedded drugs from releasing at the designed rate in the early stage. PLLA degradation profile is a function of its crystallinity, and control over surface crystallinity allows for modification of initial drug release profiles. In this study, laser irradiation is used to modify PLLA surface crystallinity, and its effect on biodegradation profile is investigated. Lower crystallinity favors water penetration into the matrix. As evaluated by molecular weight (MW) via the gel permeation chromatography and material mass change, the reduced surface crystallinity causes higher initial MW decrease rate and earlier occurrence of mass loss. An accelerated initial degradation rate and a shortened induction period of PLLA biodegradation are experimentally obtained. Wide-angle X-ray diffraction measurements show that crystallinity increases with a longer degradation period, suggesting that chain scission enhances chain mobility and thus leads to chain reorganization from a disordered to an ordered state. Based on the hydrolysis reactions and material diffusion, a model is developed to numerically investigate the effect of laser irradiation on the biodegradation profile. A reduced induction period of biodegradation gives the ability to tailor the initial drug release to achieve a designed release rate.

Introduction

Biodegradable polymers have been attracting wide attention due to their biocompatibility and biodegradability. Being biodegradable, poly(L-lactic acid) (PLLA) is now used in food packaging and tissue engineering applications. The chemical structure of PLLA makes it favorable in drug delivery because it hydrolyzes in the human body into lactic acid, which is then excreted with no toxicity. In drug delivery, drugs are embedded in a polymer matrix and released as it degrades. The advantages of using biodegradable polymers in a drug delivery system can be manifested by the controlled drug release profiles against time [1]. However, due to the induction period of polymer degradation caused by the time for water molecules to penetrate into the matrix, embedded drugs are not released at the designed rate in the early stage

PLLA degradation in a physiological environment occurs via hydrolysis, in which water penetrates into the polymer matrix, attacking the ester bonds. Water molecules readily accommodate themselves in the amorphous region, but hardly in the crystalline region, because the crystal structure is highly packed and densely ordered [2]. Therefore, the degradation rate of the ester bonds is higher in the amorphous region, and the disorientation of the lamellae and disappearance of the crystal structure occur later [3]. PLLA hydrolysis is complicated by autocatalysis [4]. Hydrolysis increases as the concentration of reaction products increases. The hydrolysis of polyester produces shorter chains with acid and alcohol end groups. The acid end groups can dissociate leading to an acidic environment, and accelerates hydrolysis. Therefore, diffusion of the shorter chains out of the polymer plays a key role in controlling the overall degradation rate. Another factor that complicates biodegradation is the increase of crystallinity during degradation [5,6]. Preferential degradation in the amorphous region leaves the crystalline material behind, leading to a mostly crystalline material. Chain scission as a result of degradation also increases chain mobility which facilitates the crystallization process in the amorphous phase.

Since change of surface crystallinity may have potential to tailor the initial PLLA degradation rate, laser irradiation as a heating source to modify the surface crystallinity has drawn increasing attention. Using the Nd:YAG laser with the photon energy lower than PLLA bond energies, the amount of PLLA crystallinity reduce has been quantified through the wide-angle X-ray diffraction (WAXD) measurements [7]. Excimer lasers operating at UV wavelengths with photon energies higher than certain bond energies in polymers have also been used to modify surface crystallinity [8,9]. It has been shown that surface crystallinity can be reduced with no measurable chemical modifications due to the low radical mobility in the crystal structure [9]. The effects of laser treatment on degradation profile, however, have not been studied.

The objective of this work is to investigate the effects of laser surface treatment on the PLLA degradation profile, characterized by the change of mass, molecular weight (MW), and crystallinity. Accelerating the initial research processes would benefit the development of this promising biomaterial. Since PLLA degradation proceeds by a similar mechanism at the elevated temperatures [10], the accelerated degradation is conducted at the elevated temperature. MW and crystallinity are determined through the gel permeation chromatography (GPC) and WAXD, respectively. A numerical model is developed to capture the degradation process.

Background

Laser Melting on Polymer

Polymer melting is an amorphization process in which crystalline polymer chains detach from crystals. Crystalline chains are held in the crystal structures by the van der Waals forces and hydrogen bonds. These weak bonds are broken during melting, leading to a less ordered structure. Melting initiates at the crystal fold surface, followed by the decrease of crystal lateral dimension. Occurring within nanoseconds [11], polymer melting induced by nanosecond laser irradiation is feasible. Crystallinity is reduced after laser melting as a result of slow crystallization kinetics when compared with the rapid melting kinetics [7-9]. Polymer absorption of photons with energies exceeding the bond energy can break the bonds. In PLA, this reaction occurs between two CH_3CHCOO units if no oxidation occurs, while the separated CH_3CHCOO units can recombine. According to the cage effect, the higher PLLA crystallinity has been shown to reduce the amount of bond breaking and lead to insignificant chemical modifications under UV laser irradiation [9].

Biodegradation of Polyester

PLA is a biodegradable polyester and degrades in the human body through hydrolysis, in which water molecules attack the ester bond via

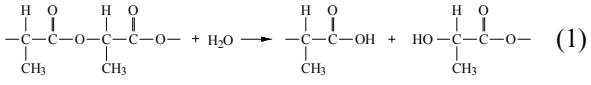

(1)

Hydrolysis causes backbone scission, and produces shorter chains with carboxylic (-COOH) groups and alcohol (-OH). The hydrolysis rate is proportional to the number of ester bonds present in each monomer constituting the polymer. The number of reactive bonds decreases as the hydrolysis process goes on. Hydrolysis rate thus depends on the molar concentrations of the monomer still present in the polymer chain, C_e, and water, C_w [12], and is represented as

$$\frac{dC_e}{dt} = -k_1 C_e C_w \tag{2}$$

The rate constant k_1 depends on temperature and does not vary with reaction. The generated carboxylic end groups have a high degree of dissociation and can act as a catalyst to accelerate the hydrolysis reaction. The hydrolysis reaction of polyesters can thus be autocatalytic if the generated carboxylic end groups remain in the bulk [13]. In this case, the reaction rate depends on the concentration of the carboxylic end groups, C_{COOH}, as well. Based on the autocatalytic scheme, the hydrolysis rate is proposed as [14]

$$\frac{dC_e}{dt} = -k_2 C_e C_w (C_{COOH})^n \tag{3}$$

where k_2 is the rate constant for the autocatalysis reaction, and n accounts for the dissociation of the carboxylic groups and can be used as an empirical parameter to reflect the reactions [15]. In the hydrolysis reaction, therefore, the concentration of the monomers C_e reduces due to chain cleavage.

Amorphous chains hydrolyze in three stages before generating monomers [16]. In stage 1, chain cleavage commences in the intact amorphous chains, resulting in the breaking of amorphous tie chains. In stage 2, chain cleavage occurs on already broken amorphous chains, creating oligomers no longer connected to any crystal. In stage 3, hydrolytic reactions occur on short amorphous segments protruding from the crystals and the oligomers produced in stage 2. The hydrolysis in this stage generates monomers which have high mobility, and can diffuse out of the matrix.

Polyester, such as PLLA, can be semicrystalline, and the amorphous region experiences a higher hydrolysis rate than the crystalline region [2,17]. This is a result of the highly packed structure in the crystalline region, which prohibits easy penetration of the water molecules. Water molecules, instead, readily diffuse through the amorphous region and accommodate themselves there, which accelerates the hydrolysis rate [2]. The hydrolysis of the amorphous region occurs randomly, but occurs preferentially on the crystal fold surfaces due to the less packed structure on the surfaces [18]. Random hydrolysis generates chains with a wide length distribution; preferential hydrolysis on fold surfaces can lead to the chains representing the integral folds the crystalline residues [17,19]. Chain scission in the amorphous region generates shorter

segments with higher mobility. Due to intermolecular hydrogen bonds and van der Waals forces, the mobile segments reorganize themselves from a disordered to an ordered state, which leads to crystallization during hydrolysis [2].

Numerical Model

A 2D symmetric model is developed to numerically investigate the effect of laser treatments on biodegradation profiles. Laser energy absorbed by the semitransparent bulk PLLA generates temperature governed by the heat equation

$$\rho C_p(T)\frac{\partial T}{\partial t} = \nabla\cdot(k\nabla T)+q(z,t) \quad (4)$$

where ρ is mass density, $C_p(T)$ is specific heat as a function of temperature T, k is thermal conductivity, $q(z,t)$ is the laser power density as a function of depth from the laser irradiated surface z and time t, expressed as

$$q(z,t)=Q_0\cdot exp(-\alpha z)\cdot exp\left[-4ln2\left(\frac{t-2t_p}{t_p}\right)^2\right] \quad (5)$$

where Q_0 is peak power density, α is absorption coefficient, t_p is pulse width. The parameters and the change in $C_p(T)$ during the phase transition are further detailed in ref. [9]. Since polymer crystals melt within a temperature span, from T_m to $T_m+\Delta T_m$, crystal fraction melts within this range is expressed as $\phi(t,T_m)dT_m$ and the total crystallinity is then $\Phi(t)=\int_{T_m}^{T_m+\Delta T_m}\phi(t,T_m)dT_m$. The change of $\phi(t,T_m)$ during melting is [20]

$$\frac{d\phi(t,T_m)}{dt} = -R_m(\Delta T)\phi(t,T_m) \quad (6)$$

The melting rate coefficient R_m is a function of superheating, $\Delta T=T-T_m$, expressed as $R_m=R_m(\Delta T)$ if $\Delta T>0$ and $R_m=0$ if $\Delta T<0$. Molecular dynamics simulations suggest that crystallinity decreases within ns, and R_m is of the order of $10^9\ s^{-1}$ [21]. The obtained crystallinity distribution as a result of laser irradiation is imported into the degradation model as the initial condition.

Biodegradation is a complicated process, and a phenomenological model can capture the key features of the degradation process and give predictions consistent with existing experimental observations [15]. The semicrystalline polymer during degradation is viewed as consisting of 7 species in the current model: non-degraded amorphous chains, degraded amorphous chains in stages 1, 2, and 3 [16], crystalline chains, monomers, and water molecules. Non-degraded and degraded amorphous chains can hydrolyze via the cleavage of the ester bonds contained in the species, but are assumed unable to diffuse due to restricted mobility. Monomers have high mobility and can diffuse. Amorphous polymer chains can crystallize during degradation. Crystalline polymer chains cannot diffuse and are assumed to hydrolyze at a rate one order of magnitude smaller than the amorphous chains [21], generating chain scission on the crystal fold surface. Water molecules are assumed to be abundant in time and space, and the size distribution of polymer chains is neglected. The generated acid end groups of the monomers also accelerate the hydrolysis through autocatalysis. The molar concentration of the non-degraded amorphous chain is thus expressed as

$$\frac{dC_a}{dt} = -k_{non,a}C_aC_w - k_{auto,a}C_aC_wC_m^n - k_a\frac{dC_c}{dt} \quad (7)$$

where C_a and C_c are the molar concentrations of monomers in the non-degraded amorphous chains and crystalline chains, respectively. C_w is the water concentration, assumed constant. The variable n accounts for the dissociation of the acid end groups, assumed unity. The first term on the right reflects non-autocatalytic hydrolysis and the second term reflects the autocatalytic hydrolysis, where $k_{non,a}$ and $k_{auto,a}$ are phenomenological rate constants, and k_a accounts for portion of the total crystallinity change due to the hydrolysis of the non-degraded amorphous chains. The hydrolysis of the non-degraded amorphous chains generates degraded amorphous chains in stage 1, which is hydrolyzed into stage 2 and contributes to crystallinity. Therefore, the monomer concentration in stage 1 is

$$\frac{dC_{as1}}{dt} = k_{non,a}C_aC_w + k_{auto,a}C_aC_wC_m^n - k_{non,as1}C_{as1}C_w - k_{auto,as1}C_{as1}C_wC_m^n - k_{as1}\frac{dC_c}{dt} \quad (8)$$

where C_{as1}, $k_{non,as1}$, and $k_{auto,as1}$ are the molar concentration of the ester bonds in the degraded amorphous chains in stage 1, and the rate constants of the two types of hydrolysis reactions for stage 1, respectively. k_{as1} accounts for portion of the total crystallinity change due to stage 1 hydrolysis. Similarly, the molar concentration of the monomers in stages 2 and 3 are

$$\frac{dC_{as2}}{dt} = k_{non,as1}C_{as1}C_w + k_{auto,as1}C_{as1}C_wC_m^n - k_{non,as2}C_{as2}C_w - k_{auto,as2}C_{as2}C_wC_m^n - k_{as2}\frac{dC_c}{dt} \quad (9)$$

$$\frac{dC_{as3}}{dt} = k_{non,as2}C_{as2}C_w + k_{auto,as2}C_{as2}C_wC_m^n - k_{non,as3}C_{as3}C_w - k_{auto,as3}C_{as3}C_wC_m^n - k_{as3}\frac{dC_c}{dt} \quad (10)$$

where C_{as2} and C_{as3} and the monomer concentrations in stages 2 and 3, and $k_{non,as2}$, $k_{auto,as2}$, $k_{non,as3}$, $k_{auto,as3}$, k_{as2}, and k_{as3} are the constants similarly defined in Eq. (8). During degradation, the crystallization of linear polyesters can be described by the Avrami equation [5], $\phi=1-exp(-k_c t^m)$ where ϕ is the fraction of monomers in the crystalline domain, k_c is the Avrami constant and m is the Avrami exponent [22]. Hydrolysis of the stage 3 species generates monomers which diffuse out of the matrix. By assuming Fick's law for monomer diffusion, the molar concentration of monomers is governed by

$$\frac{dC_m}{dt} = k_{non,as3} C_{as3} C_w + k_{auto,as3} C_{as3} C_w C_m^n + \nabla\cdot(D\nabla C_m) \quad (11)$$

where D is the monomer diffusivity.

The coupled partial differential Eqs. (4) and (6) are solved to determine crystallinity change due to laser treatments. The solutions are utilized as initial conditions to solve the coupled Eqs. (7)-(11) to capture degradation profiles. The two sets of coupled equations are solved through the finite element method in COMSOL Multiphysics 4.1.

Materials and Methods

PLLA granules were provided by PURAC and used as received. PLLA films were prepared through thermal compression under 5.7×10^4 Pa at 180°C for 4 hours, and cooled down in air. Crystals develop during the cooling process. The obtained film is around 1 mm thick. Laser treatment was conducted on both film sides by a KrF excimer laser with wavelength 248 nm and pulse width 25 ns. The homogenized excimer laser beam has a spatially uniform intensity favorable for a uniform surface treatment. The film is radiated by a single pulse in argon atmosphere with a flow rate of 15 standard cubic feet per hour to prevent oxidation. To determine film crystallinity, the WAXD measurement is performed using the Inel X-ray diffractometer. Monochromatic CuKα radiation with wavelength λ=0.15418 nm at 40 kV and 30 mA is used. X-ray photoelectron spectroscopy (XPS, PHI 5500 ESCA) is used to analyze chemical constituents of the films. The O_{1s} and C_{1s} spectra are captured, and the take-off angle is 45°.

During degradation tests, each film sample was placed in a vial and fully immersed in a 10 mL phosphate buffered saline (PBS) with a pH of 7.4 purchased from Life Technologies. The vials were placed in a water bath at 70°C, and the PBS was replaced with fresh one every two days. After degradation, the samples were dried in vacuum for two days. The film mass before and after vacuum drying was recorded. The weight-average MW (M_w) and number-average MW (M_n) of the films were determined in tetrahydrofuran (THF) with the gel permeation chromatography (GPC) at room temperature. Crystalline PLLA were first dissolved in methylene chloride and rapidly dried with a rotary evaporator to obtain the amorphous form with higher solubility in THF. PLLA/THF solutions were prepared with 1 mg/1 mL concentration for GPC measurements. Film crystallinity is determined by the WAXD, and film morphology is observed with the stereomicroscopy and optical profilometry.

Results and Discussion

Effect of Laser Irradiation on Crystallinity and Chemical Modifications

As molded film without laser treatment is not totally transparent because of crystals formed during the cooling period of the molding process. Laser treatment generates opaque spots, a result of strong light scattering from the roughened surface as observed by optical profilometry. Increased surface roughness is believed to be due to laser surface melting. The effect of laser irradiation on PLLA crystallinity is investigated via the WAXD. The WAXD peak becomes less prominent for the films treated with higher laser fluences, due to a lower crystallinity. Crystallinity can be calculated [23] with the results given in Fig. 1, which shows that the crystallinity decreases at 2.4 J/cm^2 as a result of laser melting.

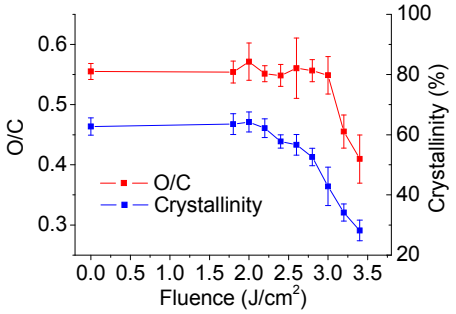

Figure 1: Crystallinity and the ratio of the O_{1s} peak area to the C_{1s} peak area of the laser treated PLLA films as a function of laser fluence. The error bar represents the standard deviation of 3 data points.

To investigate possible chemical modifications under laser irradiation, the XPS measurements are performed. Chemical reactions caused by laser irradiation with photon energies higher than the bonding energies produce small molecules such as CO and CO_2, and reduce the total ratio of oxygen to carbon [24]. The O_{1s} and C_{1s} spectra are recorded, and the ratio is shown in Fig. 1. The ratio remains constant at fluence lower

than 3.0 J/cm^2, and drops when fluence reaches 3.2 J/cm^2, indicative of chemical modifications due to laser irradiation. PLLA film remains chemically unmodified below 3.0 J/cm^2 due to the cage effect, which states that the free radicals generated by the dissociation of molecules cannot move apart because of the confinement of surrounding molecules [9]. This results in the recombination of the dissociation products, which then return to the initial state. The critical fluence of 3.0 J/cm^2 causes the maximum crystallinity decrease with insignificant chemical modifications, and is used as the energy level to treat the films in this study.

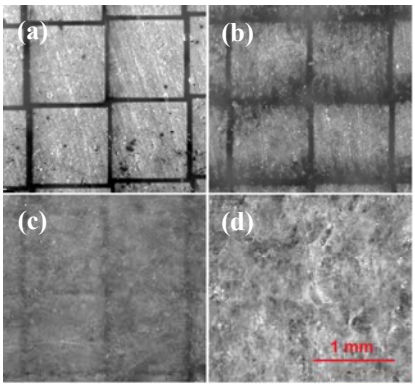

Figure 2: Surface morphology of the laser treated film (a) before and after degradation for (b) 3 days, (c) 8 days, and (d) 14 days under the stereomicroscope. The squares in (a) are laser spots. The laser spots become less prominent in the early stage of degradation, suggesting the degradation of the laser melted layer. Degradation in the non-melted volume occurs in the later stage of degradation.

Effects of Laser Irradiation on Degradation

Modification of Morphology A laser treated sample degraded for 14 days is shown in Fig. 2. A uniformly opaque morphology is observed while the laser spots become unclear. Further morphology investigations are given by stereomicroscopic images of the laser treated sample as a function of degradation period in Fig. 2. Laser treated film before degradation in given in Fig. 2(a). The 1mm×1mm square spot is generated by laser irradiation. As degradation progresses, spot edges become less well defined, suggesting the degradation of laser melted layer, as shown in Fig. 2(b) for 3-day degradation. After 8 days, Fig. 2(c), spot edges are indistinct and the gaps between spots are opaque a result of higher crystallinity developed during degradation. During prolonged testing, the effect of laser melted layer becomes less significant and degradation in the non-melted volume occurs. Eventually, the laser spots and edges disappear, Fig. 2(d), and the film morphology is similar to that of the non-laser treated film after the same degradation period. It is observed that light scattering is not uniform over the surface. Surface roughness is caused by the selective degradation on the amorphous region, leaving the crystalline region with strong local light scattering.

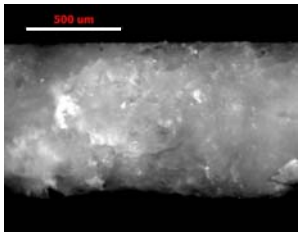

Figure 3: Cross section of the laser-treated film degraded for 14 days. The bulk remains solid, suggesting that the autocatalytic degradation is less dominant.

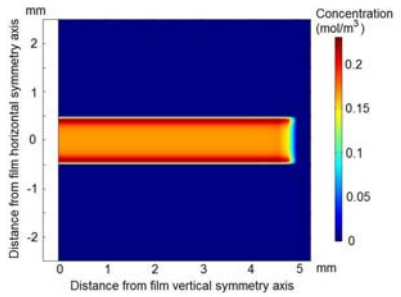

(a) Degraded for 0.5 days

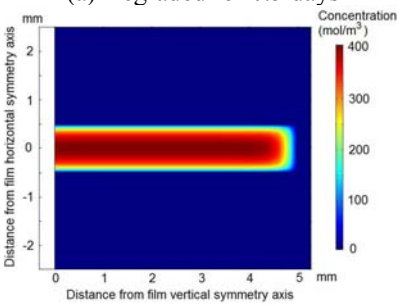

(b) Degraded for 6 days

Figure 4: Simulated spatial distribution of monomer concentration in the laser treated film degraded for (a) 0.5 days and (b) 6 days.

The cross section of the laser treated film after 14-day degradation is given in Fig. 3. It is observed that the bulk remains solid, which suggests that autocatalytic degradation is less dominant as a result of easy diffusion of acidic monomers out of the film. Spatial degradation profiles are given in Fig. 4, which illustrates the spatially resolved molar concentration of the monomers. The concentration after 0.5-day degradation, based on the calculated value of laser

melted layer with thickness of 80 μm is shown in Fig. 4. The monomer concentration on the surface is higher than that in the bulk, suggesting the accelerated degradation in the laser melted layer. In the later stage of degradation, Fig. 4(b), the monomer concentration in the non-melted volume starts to increase, which signifies that laser melted layer experiences a higher degradation rate, as agreed with the optical observation discussed in Fig. 2.

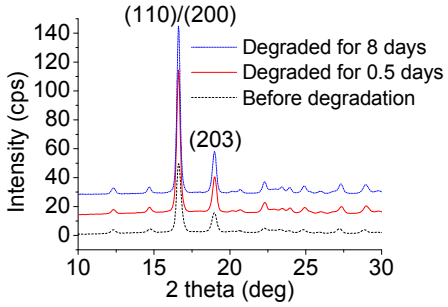

(a) Non-laser treated film

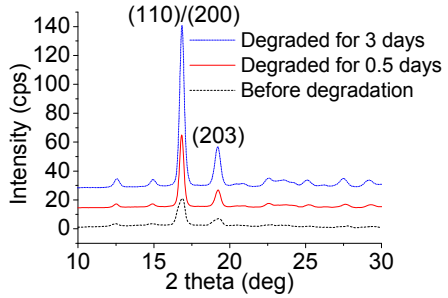

(b) Laser treated film

Figure 5: WAXD profiles for the (a) non-laser treated and (b) laser treated films after different degradation periods. Peak intensity increases with degradation period, suggesting a higher crystallinity. Profiles are shifted in y direction for viewing clarity.

Modification of Crystallinity The WAXD measurements have been conducted to investigate crystallinity modifications during degradation, with results given in Fig. 5 for the non-laser treated and laser treated films. Laser treatments cause surface melting and a reduced peak. For both films, the peaks become more prominent with longer degradation period, suggesting the occurrence of crystallization during degradation. Crystallinity calculations [23] given in Fig. 6 show that crystallinity increases with degradation period, in agreement with Fig. 5. For both films a significant increase of crystallinity is observed at day 0.5, when the sample MW begins to decrease, as will be discussed in the section below. The decrease of MW renders chain mobility and favors chain reorganizing and crystallization. The larger amount of amorphous region in the beginning also contributes to the higher rate of crystallization, as predicted by the Avrami crystallization theory [25]. Crystallization slows between day 0.5 and day 5 for the non-laser treated film, because part of the amorphous chains is less crystallizable, including the rigid amorphous phase (RAP) [26] and entangled chains. Both hinder chain movements and make it difficult for the chains to relax and crystallize. Another significant crystallinity increase occurs at day 8 for the non-laser treated film, and day 3 for the laser treated film. This crystallinity increase corresponds to the initiation of mass loss, Fig. 11. It is suggested that the crystallinity increase at this stage is mainly caused by the loss of amorphous chains.

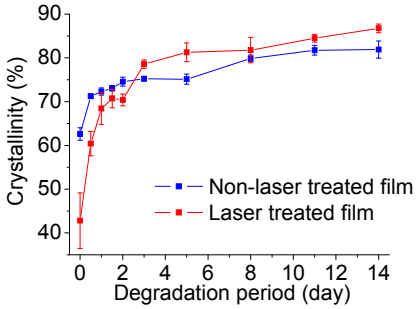

Figure 6: Crystallinity as a function of degradation period determined from the WAXD for the laser treated and non-laser treated films. Crystallinity increases with the degradation period. A significant increase occurs on day 0.5 for both films. Another increase is observed on day 8 for the non-laser treated film and day 5 for the laser treated film. The error bar represents the standard deviation of 3 data points.

Modification of Molecular Weight and Film Mass Film degradation profiles are characterized by sample MW and film mass. The MW distributions as a function of degradation period are given in Fig. 7 for both non-laser treated and laser treated films. The y-axis plots the mass fraction of chains (w) per increment of MW in a logarithmic scale (logM). The number average MW (M_n) and weight average MW (M_w) are determined from the MW distributions. The polydispersity index (PDI), defined as M_w/M_n, is also calculated as a measure of distribution of MW. M_n, M_w, and PDI for the non-laser treated and laser treated films are given in Fig. 8. Film mass as a function of degradation period is given in Fig. 9. Simulated sample MW and film mass for both films are given in Figs. 10 and 11.

For the non-laser treated film, the GPC profile before degradation is centered at around 120000 g/mol and the distribution is narrow, as shown in Fig. 7(a). As the degradation period increases, days 2, 3 and 5, the distribution gradually becomes wide and moves to the

left. A small hump is developed at around 60000 g/mol at day 5. Sample MW decreases as given in Fig. 8(a), which also shows an increasing PDI as a result of random chain scission. Random chain scission before day 5 occurs in the amorphous region, causing the chains to degrade into segments with various MWs [17]. There is no obvious mass decrease before day 5 for non-laser treated film, as given in Fig. 9, because the degraded segments are not small enough to diffuse out of the film. The degraded segments have better mobility, and reorganize themselves from a disordered to an ordered state as a result of intermolecular hydrogen bonds and van der Waals force during the degradation period, which increases the crystallinity for the first 5 days of degradation, as shown in Fig. 6.

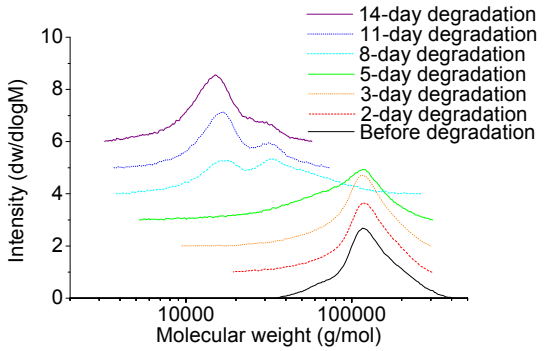

(a) Non-laser treated film

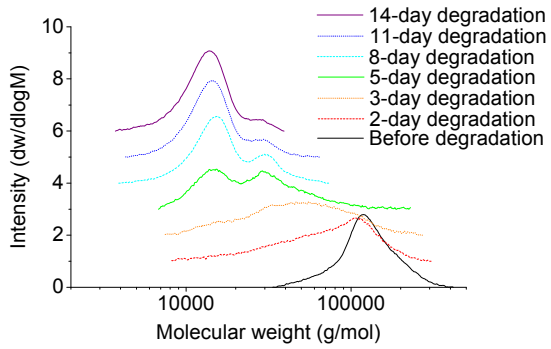

(b) Laser treated film

Figure 7: GPC profiles of the (a) non-laser treated and (b) laser treated films after the designed degradation periods. For (a), the distribution becomes wider and moves to the left as the degradation period increases to day 5, representing the random chain scission in the amorphous region. After day 8, a distinct new peak is developed due to selective chain scission of the fold surface of crystals. For (b), the MW distribution extends to the left before day 3, signifying the random chain scission of the laser melt layer. At day 5, two distinct peaks are developed due to the selective chain scission of the partially melted crystal fold surfaces. Profiles are shifted in y direction for viewing clarity.

At day 8, the GPC profile of the non-laser treated films moves to the left significantly, Fig. 7(a). A distinct peak, corresponding to a smaller MW of 10300 g/mol, is developed. This is not caused by random scission, but is due to the selective scission of the crystal fold surface. This preferential scission generates chains with MW representing the integral folds the crystalline residues [17,19]. The left peak is thus mainly composed of the MW of the crystalline residues, and the right peak mainly comes from the amorphous region experiencing random chain scission. As degradation approaches to 11 and 14 days, the right peak starts to diminish due to the continuous scission of amorphous chains, and the overall distribution is mainly composed of a peak centered at 10300 g/mol. The PDI thus decreases, as shown in Fig. 8 (a).

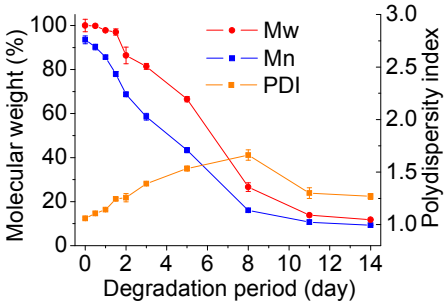

(a) Non-laser treated film

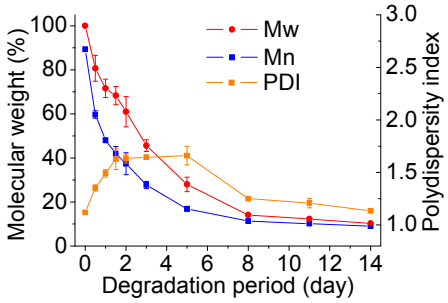

(b) Laser treated film

Figure 8: M_w, M_n, and PDI of the (a) non-laser treated and (b) laser treated films after the designed degradation periods. M_w and M_n decrease at a higher rate for the laser treated films, as a result of fast degradation of the laser melted layer. The non-homogeneous degradation of the melted layer and bulk leads to a larger PDI. The error bar represents the standard deviation of 3 data points.

The smallest MW, around 3000 g/mol, is detected after day 8 in Fig. 7(a), while Fig. 9 shows that mass decrease also occurs at day 8. This suggests that chains with MW smaller than 3000 g/mol are diffused out of the film. Figure 6 shows that crystallinity increases significantly at day 8 for the non-laser treated film. Thus, the materials diffusing out of the film are

mainly amorphous. The reduction of amorphous material increases the crystallinity in the film and also leads to clearer local light scattering shown in Fig. 2(d).

The GPC profiles of the laser treated film are given in Fig. 7(b). Before degradation, the GPC profile of the laser treated film is centered at 120000 g/mol with the profile shape similar to the non-laser treated film. Laser treatments are not shown to affect PLLA MW. When compared with the non-laser treated film, MW decreases at a high rate at the early stage for the laser treated film. On days 2 and 3, significant changes of GPC profiles are observed in Fig. 7(b). At day 2, the original peak intensity decreases, while the distribution extends to the smaller MW region. The original peak diminishes at day 3, and a hump at smaller MW region is developed. During this period, a random chain scission of the laser melted layer occurs. Non-homogeneous degradation at the laser melted layer and the bulk widens the MW distribution and thus increases the PDI, Fig. 8(b). The high degradation rate of the laser treated film is a result of easy water molecule penetration into the laser melted layer, which possesses a less ordered structure. The faster water penetration into the bulk is also responsible for the diminished original peak at day 3.

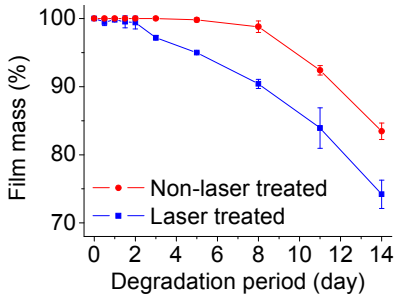

Figure 9: Experimental results of film mass with and without laser treatments. Mass decrease is clearly observed after day 8 for non-laser treated film and after day 3 for laser treated film. The error bar represents the standard deviation of 3 data points.

At day 5, the hump is split into two peaks for the laser treated film, as shown in Fig. 7(b). The distinct distribution of two peaks suggests that the selective chain scission on the crystal fold surface commences. This phenomenon is observed in the non-laser treated film at day 8. The earlier occurrence of this selective scission for the laser treated film can be due to the less ordered structure of the partially melted crystals. For partially melted crystals, the crystal thickness is diminished, which increases the molecular loop length on the fold surface [27].

This longer loop length allows for larger free volume for water molecules to penetrate, and facilitates hydrolysis on the fold surface. Toward the late stage of the degradation period, shown in Fig. 7(b), the right peak diminishes and the left peak increases. This left peak is composed of the chains with MW representing the integral folds the crystalline residues, as well as the smallest MW distribution of chains which can remain in the matrix. The narrowing MW distribution at the late degradation stage decreases the PDI, as given in Fig. 8(b) after day 5.

Accelerated initial degradation of the laser treated film leads to shorter induction periods of mass loss, which occurs at day 3, compared to day 8 for the non-laser treated film as shown in Fig. 9. Similar to the non-laser treated film, the decrease of film mass is accompanied with the increase of crystallinity, as given in Fig. 6. This again reflects the fact that the initial mass loss comes from the diffusion of the degraded amorphous chains from the matrix. The laser melted layer is composed of a larger amount of amorphous chains, part of which degrades and diffuses out at a higher rate, while part of which crystallizes as the chains do in the bulk. The laser melted material degrades with reducing MW before day 3, and its diffusion process happens around day 3. Eventually, the effect of laser melted layer on degradation is lost. The sample MW and film mass decrease at similar rates as the non-laser treated film, as observed in Figs. 8 and 9 respectively.

Simulation results of the MW change are given in Fig. 10. As agreed with experiments, the laser treated film experiences a larger MW decrease. The difference stems from a decreased rate at the early stage of degradation of the laser melted layer, while the rates become similar afterwards. Experimentally, the MW of the non-laser treated film does not decrease as significantly as in simulation before day 1. This can be a result of the time required for water penetration in experiments, which is not considered in simulation and causes the overestimation of the MW decrease.

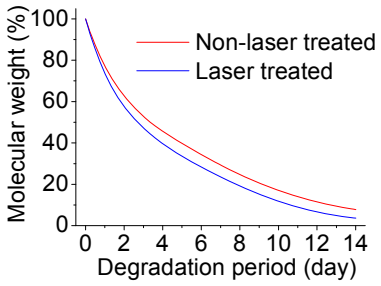

Figure 10: Simulation results of the molecular weight of the non-laser treated and laser treated films.

The simulated mass change of both films is given in Fig. 11. The result captures the phenomenon that film mass decrease after an induction period. During the induction period the original amorphous polymer chains degrade into fragments not small enough for diffusion out of the film. Once the fragments experience further degradation into monomers, they can diffuse and leads to mass decrease. Experimentally, the mass change is more significant when compared with simulation, as a result of the fragmentation and erosion of crystalline material from the surface during degradation, as the monomers diffuse out of the matrix [28]. The effect of crystallinity loss in materials is not considered in simulation, leading to a conservative prediction.

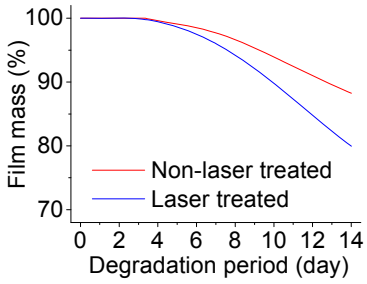

Figure 11: Simulation results of the film mass with and without laser treatments.

Conclusions

The effect of laser irradiation on PLLA biodegradation profile has been studied experimentally and numerically. Laser irradiation melts the material surface. The melted layer has lower crystallinity yet no observable chemical changes according to the WAXD and XPS measurements. Optical observations and simulation show that degradation initiates on the film surface, and the melted layer allows for the accelerated initial degradation rate. The GPC measurements show that the laser treated film experiences a higher initial MW decrease rate, which leads to a shorter induction period of mass loss in the laser treated film. Multiple peaks in the GPC profiles are observed in both laser treated and non-laser treated films, demonstrating the heterogeneous degradation in the amorphous and crystalline regions. For the laser treated film, the multiple-peak profile is observed at the earlier stage, suggesting that laser treatment may also disorder the crystal fold surface, leading to an easier local chain scission. Chain scission during the degradation period allows for chain reorganization from a disordered to an ordered state. The WAXD measurements demonstrate that, although beginning with a lower crystallinity, the laser treated film ends up with a higher crystallinity, as a result of higher degradation rate and thus higher chain mobility. Changes of MW and film mass are captured by the simulation results, which also demonstrate the distinct species evolution profiles during degradation in the laser treated and non-laser treated films. The modified biodegradation profiles through laser irradiation potentially give the ability to tailor the initial drug release to achieve a designed release rate.

Acknowledgements

Financial support from NSF under CMMI-1030536 is acknowledged. WAXD and XPS measurements were carried out at MRSEC, Columbia University.

References

[1] Amass, W., Amass, A. & Tighe, B. (1998) A review of Biodegradable Polymers: Uses, Current Developments in the Synthesis and Characterization of Biodegradable Polyesters, Blends of Biodegradable Polymers and Recent Advances in Biodegradation Studies, Polym. Int. 47, 89-144.

[2] Chu, C. C. (1981) Hydrolytic Degradation of Polyglycolic Acid: Tensile Strength and Crystallinity Study, J. Appl. Polym. Sci. 26, 1727-1734.

[3] Tsuji, H. & Ikada, Y. (1998) Properties and Morphology of Poly(L-Lactide). II. Hydrolysis in Alkaline Solution, J. Polym. Sci., Part A: Polym. Chem. 36, 59-66.

[4] Siparsky, G. L., Voorhees, K. J. & Miao, F. (1998) Hydrolysis of Polylactic Acid (PLA) and Polycaprolactone (PCL) in Aqueous Acetonitrile Solutions: Autocatalysis, J. Environmental Polym. Degrad. 6, 31-41.

[5] Zong, X. H., Wang, Z. G., Hsiao, B. S., Chu, B., Zhou, J. J. & Jamiolkowski, D. D. (1999) Structure and Morphology Changes in Absorbable Poly(glycolide) and Poly(glycolide- co-lactide) during in Vitro Degradation, Macromol. 32, 8107-8114.

[6] Renouf-Glausera, A. C., Roseb, J., Farrarb, D. F. & Cameron, R. E. (2005) The Effect of Crystallinity on the Deformation Mechanism and Bulk Mechanical Properties of PLLA, Biomaterials 26, 5771-5782.

[7] Bhatla, A. & Yao, Y. L. (2009) Effect of Laser Surface Modification on the Crystallinity of Poly(L-Lactic Acid), J. Manuf. Sci. Eng. 131, 051004.

[8] Dunn, D. S. & Ouderkirk, A. J. (1990) Chemical and Physical Properties of Laser-Modified Polymers, Macromol. 23, 770-774.

[9] Hsu, S.-T., Tan, H. & Yao, Y. L. (2012) Effect of Excimer Laser Irradiation on Crystallinity and Chemical Bonding of Biodegradable Polymer, Polym. Degrad. Stab. 97, 88-97.

[10] Weir, N. A., Buchanan, F. J., Orr, J. F., Farrar, D. F. & Dickson, G. R. (2004) Degradation of Poly-L-Lactide. Part 2: Increased Temperature Accelerated Degradation, Proc. Instn. Mech. Engrs., Part H: J. Eng. in Med. 218, 321-330.

[11] Yamamoto, T. (2010) Molecular Dynamics of Reversible and Irreversible Melting in Chain-Folded Crystals of Short Polyethylene-Like Polymer, Macromol. 43, 9384-9393.

[12] Pitt, C. G. & Gu, Z. (1987) Modification of the Rates of Chain Cleavage of Poly(ε-Caprolactone) and Related Polyesters in the Solid State, J. Controlled Release 4, 283-292.

[13] Li, S. M., Garreau, H. & Vert, M. (1990) Structure-Property Relationships in the Case of the Degradation of Massive Poly(α-Hydroxy Acids) in Aqueous Media: Part 2 Degradation of Lactide-Glycolide Copolymers: PLA37.5GA25 and PLA75GA25, J. Mater. Sci.: Mater. Med. 1, 131-139.

[14] Lyu, S., Schley, J., Loy, B., Lind, D., Hobot, C., Sparer, R. & Untereker, D. (2007) Kinetics and Time-Temperature Equivalence of Polymer Degradation, Biomacromol. 8, 2301-2310.

[15] Wang, Y., Pan, J., Han, X., Sinka, C. & Ding, L. (2008) A Phenomenological Model for the Degradation of Biodegradable Polymers, Biomater. 29, 3393-3401.

[16] Stephens, C. H., Whitmore, P. M., Morris, H. R. & Bier, M. E. (2008) Hydrolysis of the Amorphous Cellulose in Cotton-Based Paper, Biomacromol. 9, 1093-1099.

[17] Tsuji, H. & Tsuruno, T. (2010) Accelerated Hydrolytic Degradation of Poly(L-Lactide)/Poly(D-Lactide) Stereocomplex up to Late Stage, Polym. Degrad. Stab. 95, 477-484.

[18] Tsuji, H. & Ikarashi, K. (2004) In Vitro Hydrolysis of Poly(L-Lactide) Crystalline Residues as Extended-Chain Crystallites: II. Effects of Hydrolysis Temperature, Biomacromol. 5, 1021-1028.

[19] Fischer, E. W., Sterzel, H. J. & Wegner, G. (1973) Investigation of the Structure of Solution Grown Crystals of Lactide Copolymers by Means of Chemical Reactions, Kol.-Z.u.Z. Polymere 251, 980-990.

[20] Toda, A., Tomita, C., Hikosaka, M. & Saruyama, Y. (1998) Melting of Polymer Crystals Observed by Temperature Modulated D.S.C. and Its Kinetic Modeling, Polym. 39, 5093-5104.

[21] Li, H., Nie, W., Deng, C., Chen, X. & Ji, X. (2009) Crystalline Morphology of Poly(L-Lactic Acid) Thin Films, Eur. Polym. J. 45, 123-130.

[22] Avrami, M. (1941) Granulation, Phase Change, and Microstructure: Kinetics of Phase Change. III, J. Chem. Phys. 9, 177-184.

[23] Alexander, L. E. (1969) X-ray diffraction methods in polymer science, John Wiley & Sons, New York.

[24] Inagaki, N., Narushima, K., Tsutsui, Y. & Ohyama, Y. (2002) Surface Modification and Degradation of Poly(Lactic Acid) Films by Ar-Plasma, J. Adhes. Sci. Technol. 16, 1041-1054.

[25] Avrami, M. (1939) Kinetics of Phase Change. I: General Theory, J. Chem. Phys. 7, 1103-1112.

[26] Menczel, J. & Wunderlich, B. (1981) Heat Capacity Hysteresis of Semicrystalline Macromolecular Glasses, J. Polym. Sci.: Polym. Lett. Ed. 19, 261-264.

[27] Belyayev, O. F. (1988) Mechanism of Melting of Oriented Polymers, Polym. Sci. U. S. S. R. 30, 2545-2552.

[28] Lam, C. X. F., Savalani, M. M., Teoh, S. H. & Hutmacher, D. W. (2008) Dynamics of *in Vitro* Polymer Degradation of Polycaprolactone-Based Scaffolds: Accelerated versus Simulated Physiological Conditions, Biomed. Mater. 3, 034108.

Meet the Authors

Shan-Ting Hsu received his B.S. and M.S. from National Taiwan University. He is currently a doctoral student at the Manufacturing Research Laboratory at Columbia University.

Huade Tan received his B.S. from Boston University and M.S. from the University of Notre Dane. He is currently a doctoral student at the Manufacturing Research Laboratory at Columbia University.

Dr. Y. Lawrence Yao is currently a professor of Columbia University's Mechanical Engineering Department and director of the Manufacturing Research Laboratory. He received his Ph.D. from the University of Wisconsin-Madison in 1988.